Supporting Information

Silver Single Atom in Polymeric Carbon Nitride as a Stable and Selective Oxygen Reduction Electrocatalyst towards Hydrogen Peroxide Synthesis

Akanksha Gupta[1,#], Manoj Shanmugasundaram[1,2,#], Shilendra Kumar Sharma[3], Sudip Chakraborty[3], David Zitoun[1,2]

[1] Department of Chemistry, Bar-Ilan University, Ramat-Gan 5290002, Israel

[2] Bar-Ilan Nanotechnology and Advanced Materials Institute, Bar-Ilan University, Ramat-Gan 5290002, Israel

[3]Materials Theory for Energy Scavenging (MATES) Lab, Department of Physics, Harish-Chandra Research Institute (HRI) Allahabad, A C.I. of Homi Bhabha National Institute (HBNI), Chhatnag Road, Jhunsi, Prayagraj (Allahabad) 211019, India

Experimental Section

Material and Methods

Chemicals and reagents

Melamine (MA, 99%), cyanuric acid (CA, 99%), citric acid (CTA, 99.5%), and silver nitrate ($AgNO_3$, 99.0%) were procured from Sigma-Aldrich. Nafion (perfluorinated resin solution, 5%, Aldrich), potassium hydroxide (pellets for analysis, EMSURE), potassium bicarbonate (CHEM-IMPEX), 2-propanol (HPLC grade, AR-b, Bio-Lab Ltd.), and absolute ethanol (dehydrated, AR-b, Bio-Lab Ltd.) were used in the study. All chemicals and reagents were used directly as received without any additional purification.

[#] Equal contribution

Synthesis of Ag-PCN

For the synthesis of Ag-PCN, melamine (MA, 10 mmol) and cyanuric acid (CA, 9.5 mmol) were dissolved separately in ultrapure water under heating at 80ºC to obtain homogeneous solutions, designated as solutions A and B, respectively. Citric acid (CTA, 0.5 mmol) and silver nitrate ($AgNO_3$, 0.25 mmol) were dissolved in ultrapure water to prepare solution C. Subsequently, solution C was added dropwise to solution B under continuous stirring for 10 minutes. The resulting mixture of solutions B and C was then introduced into solution A, and the combined solution was stirred for 4 hours at room temperature. The resulting supramolecular complex was isolated by centrifugation, washed three times with deionized water, followed by a single wash with ethanol, and dried overnight at 80°C. The dried supramolecule was then pyrolysis at 550°C under a nitrogen atmosphere for 4h, with a controlled heating rate of $10°C \cdot min^{-1}$. The final product, a yellow powder denoted as Ag-PCN. A series of Ag-PCN materials with varying silver loadings were also synthesized by adjusting the initial concentration of $AgNO_3$ during the preparation.

Synthesis of PCN

The PCN was synthesized following the same procedure as Ag-PCN, with the exception that $AgNO_3$ was not added during the preparation.

Material Characterization

The morphology of Ag-PCN and PCN were obtained from High resolution scanning electron microscopy (HRSEM), Transmission electron microscopy (TEM), images were recorded by JEM2100 JEOL instrument. To analyze and confirm the formation of atomically dispersed Ag atom sites in PCN framework, High angle annular dark field-scanning transmission electron microscope (HAADF-STEM) FEI TITAN transmission electron microscope (TEM) operated at

300 kV. The amount of metal deposited in PCN framework was analyzed via ICP-AES (Ultima-2 spectrometer; Jobin Yvon Horiba). The X-ray diffraction pattern of Ag-PCN and were recorded with a Brucker D8 Advanced X-Ray diffractometer, using Cu Kα radiation. The X-ray photoelectron spectroscopy (XPS) measurements were performed by Nexsa X-ray photoelectron spectrometer system (Thermo scientific) with a monochromates Al kα X-ray source.

Electrocatalytic Measurement

All electrochemical measurements were conducted in a standard three-electrode cell equipped with a rotating ring-disk electrode (RRDE, Pine Instruments) and a Biologic electrochemical workstation. The RRDE served as the working electrode, comprising a glassy carbon disk (geometric area: 0.2475 cm^2) and a platinum ring (geometric area: 0.1815 cm^2). A graphite rod and a Hg/HgO electrode were used as the counter electrode and reference electrode, respectively. For the working electrode preparation, the catalyst ink was prepared by dispersing 2 mg of catalyst in a solution containing 950 µL of isopropanol and 50 µL of Nafion solution. The mixture was sonicated for 1 hour to achieve a homogeneous dispersion. Subsequently, 10 µL of the catalyst ink was deposited onto a cleaned 5 mm glassy carbon disk of the RRDE. The electrode was rotated at 300 rpm for 15 minutes to ensure uniform distribution and then dried naturally at room temperature. All the catalysts loadings were maintained to be ~ 80 µg cm^{-2}. Oxygen reduction reaction (ORR) measurements were carried out in two different electrolytes: 0.1 M KOH and 0.1 M $KHCO_3$. Linear sweep voltammetry (LSV) was performed at on rates of 625 rpm, 900 rpm, 1225 rpm, 1600 rpm, 2025 rpm and 2500 rpm in an O_2 saturated electrolyte. The potential applied for obtaining the ring current of the RRDE during H_2O_2 production is 1.38V versus RHE. The H_2O_2 selectivity and the electron transfer number (n) on the RRDE of the electrocatalysts were calculated based on the equation below.

$$H_2O_2\% = \frac{2I_R/N}{I_D + (I_R/N)} \times 100\%$$

$$n = 4 \times \frac{I_D}{I_D + (I_R/N)}$$

Where I_D and I_R are the background-corrected disk and ring currents, and N is the collection efficiency (0.37) of the platinum ring determined by measuring the redox of hexacyanoferrate ($Fe(CN)_6]^{3-}$/$[Fe(CN)_6]^{4-}$).

H_2O_2 concentration measurement

The potassium iodide titration method is used to determine the amount of H_2O_2. By mixing the known amount of commercial H_2O_2 with a mixed solution containing 0.1M potassium hydrogen phthalate and 0.1M potassium Iodide and then measuring the absorbance of the mixed solution at a wavelength of 350 nm using an ultraviolet-visible spectrophotometer, a standard curve between the H_2O_2 concentration and absorbance.

H_2O_2 production in typical H-cell

The production of H_2O_2 is carried out in a two typical-chamber, three-electrode H-type electrolytic cell separated by a proton exchange membrane. Each compartment filled with 45 mL of 0.1M $KHCO_3$ solution with continuous O_2 purging. An Ag/AgCl electrode and glassy carbon rod used as the reference electrode and counter electrode. The working electrode is drop-casted with different catalyst inks onto a 1.0 x 1.0 cm^2 commercial carbon paper, with the catalysts loading of ~ 0.250mg cm^{-2}. The chronoamperometry tests were carried out at fixed potential 0.42V vs RHE. Then, the amount of H_2O_2 produced determined by the Potassium Iodide titration method.

Computational Methodology

Density functional theory (DFT) based electronic structure calculations were performed to study the reaction mechanism of two-electron transfer H_2O_2 production on Ag single atom catalyst on polycrystalline C_3N_4 monolayer [1-2]. We considered 221 supercell of pristine C_3N_4 monolayer to explore all possible binding sites in heptazine ring to accommodate the single Ag atom with 18 Angstrom vacuum in z-direction to avoid collapse of parallel periodic images. We utilized Perdew Burke Erzernhof (PBE) exchange correlation functional in conjunction with projected augmented wave (PAW) formalism in all calculations [3-4]. Spin-polarized calculations were performed by exploiting Vienna *ab-initio* simulation package (VASP) [5-6]. Plane wave basis set energy cut off 500 eV and a Gamma centered 4x4x1 kpoints Brillouin zone sampling were utilized for geometry optimization and further adsorption free energy calculations [7]. Grimme dispersion-corrected DFT-D3 methodology was exploited throughout the calculations to account the Van der Wall dispersion forces between adsorbate and C_3N_4 monolayer [8]. Energy convergence and force convergence criteria were kept 10^{-5} eV and -0.01 eV/Å respectively. Structures visualizations and images generation were performed by VESTA software [9]. Formation energy of Ag adsorbed/supported system and adsorbate *OOH adsorption energy were calculated according to equation (1) and (2) respectively [1–4]:

Formation energy was calculated by utilizing the following given formula:

$E_f = E_{total} – E_{C3N4} - E_{ag}$ ..... (1)

Where E_f = the formation energy of Ag adsorbed/support C_3N_4 (221 supercell)

E_{total} = the total energy after Ag adsorbed/support in C_3N_4 (221 supercell)

E_{C3N4} = the total energy of C_3N_4 (221 supercell)

E_{Ag} = energy of isolated single Ag atom

Adsorption energy of *OOH was calculated by utilizing the given formula:

$E_{ads} = E_{total} - E_{surface} - E_{adsorbate}$ ..... (2)

E_{ads}= Adsorption Energy of the adsorbate molecule (*OOH)

E_{total}= Total energy of the molecule adsorbed on the C_3N_4 monolayer

$E_{surface}$= Energy of the pristine C_3N_4 monolayer

$E_{adsorbate}$ = Adsorbate (OOH) molecule energy

Adsorption free energy at standard O_2 reduction potential i.e. 0.7 V~ RHE has been calculated by considering computational hydrogen electrode (CHE) model with following relation :

$\Delta G_{*OOH} = E_{ads} + \Delta ZPE - T\Delta S - eU$ ..... (1)

Where ΔG_{*OOH}, E_{ads}, ΔZPE, $T\Delta S$, and U are the change in adsorption free energy (eV) of *OOH, adsorption energy of the OOH* (E_{ads}), zero point energy correction, entropic contribution (T= 298.15 K), and applied potential respectively.

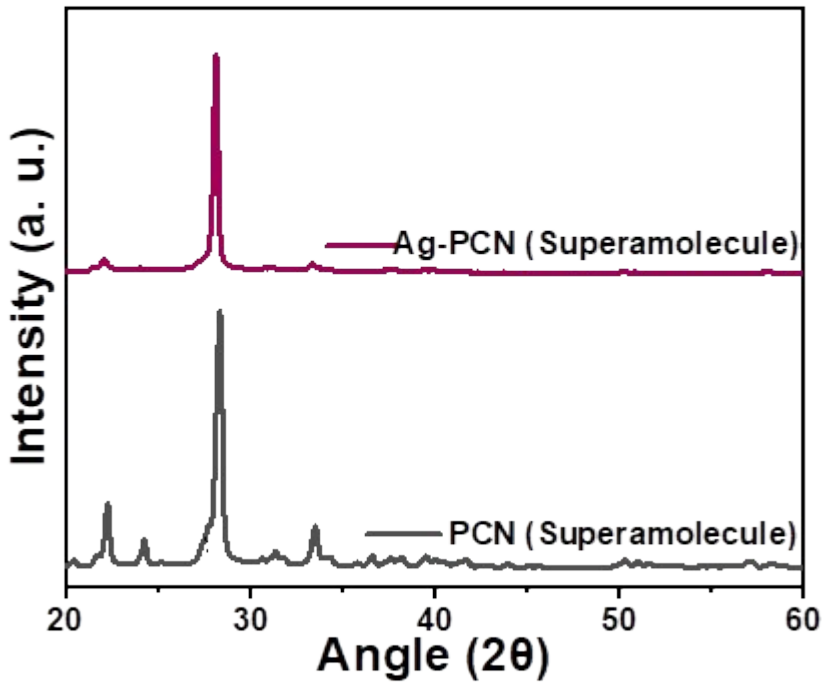

Figure S1. XRD spectra of Supramolecular.

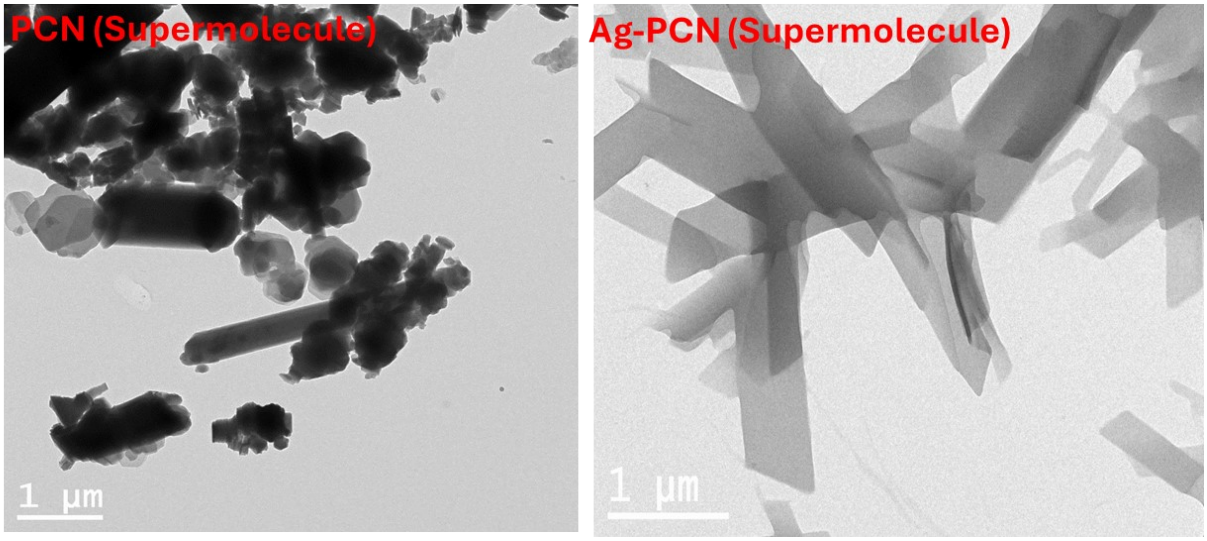

Figure S2. TEM images of PCN precursor supermolecules.

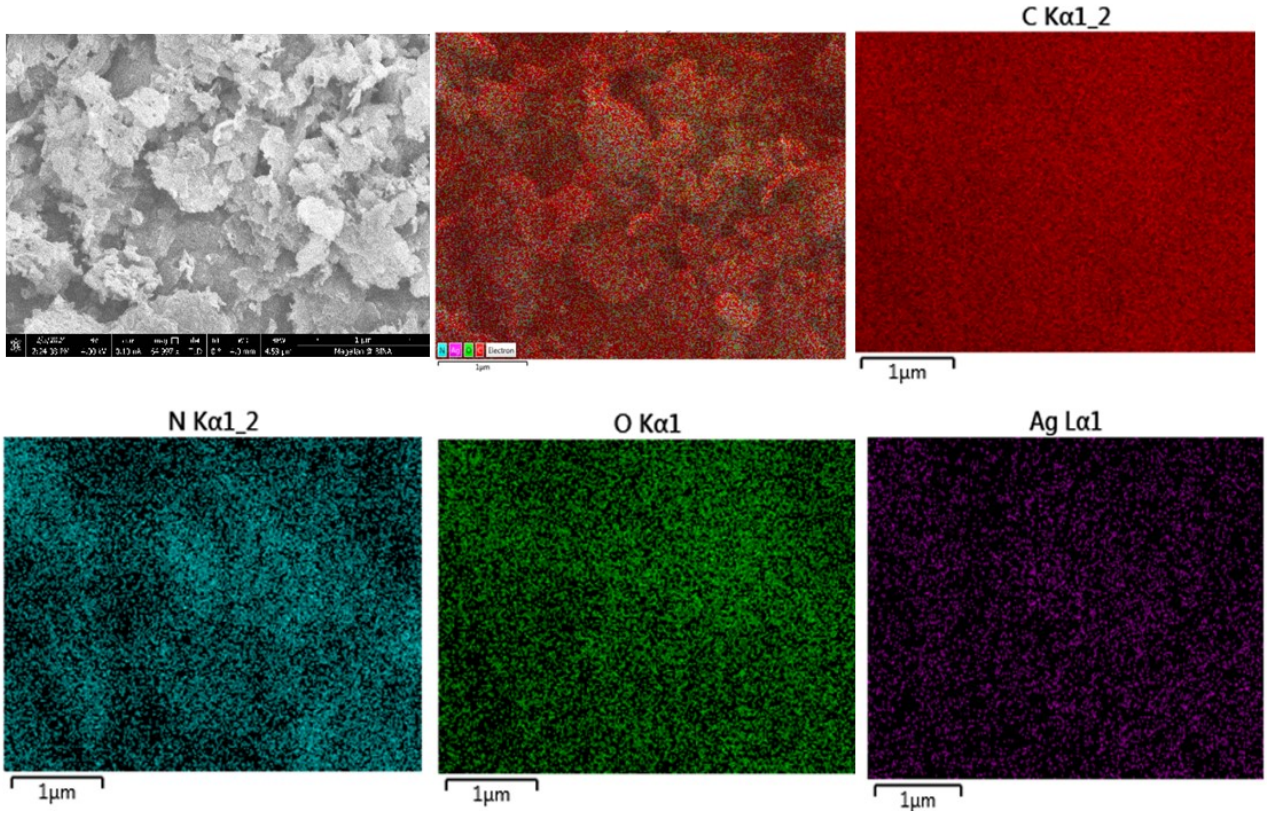

Figure S3. HRSEM image and EDS mapping of Ag-PCN.

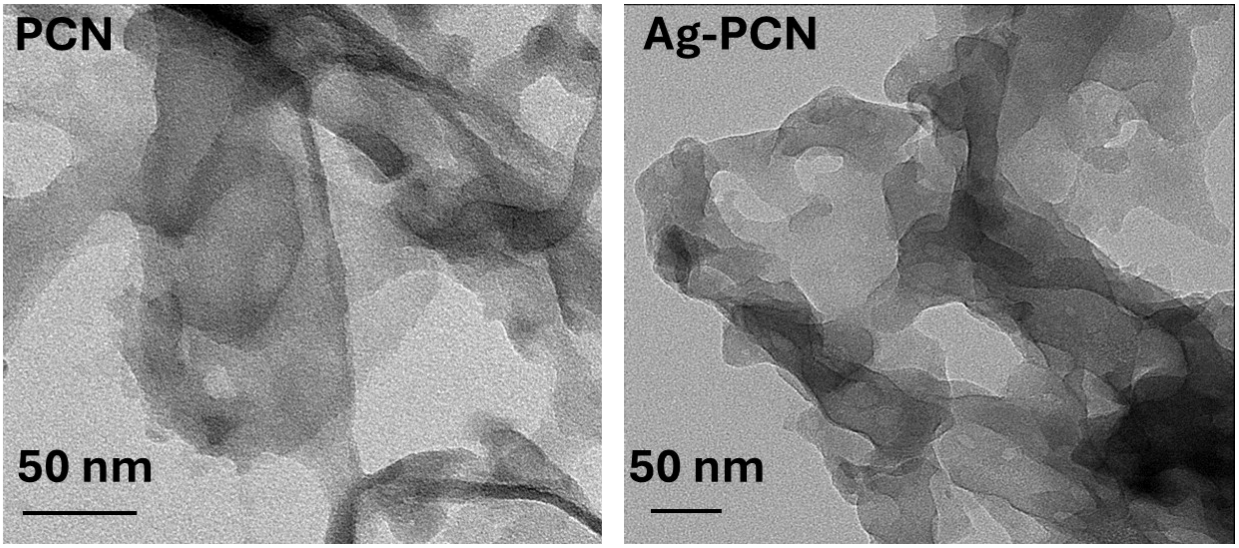

Figure S4. TEM images of PCN and Ag-PCN.

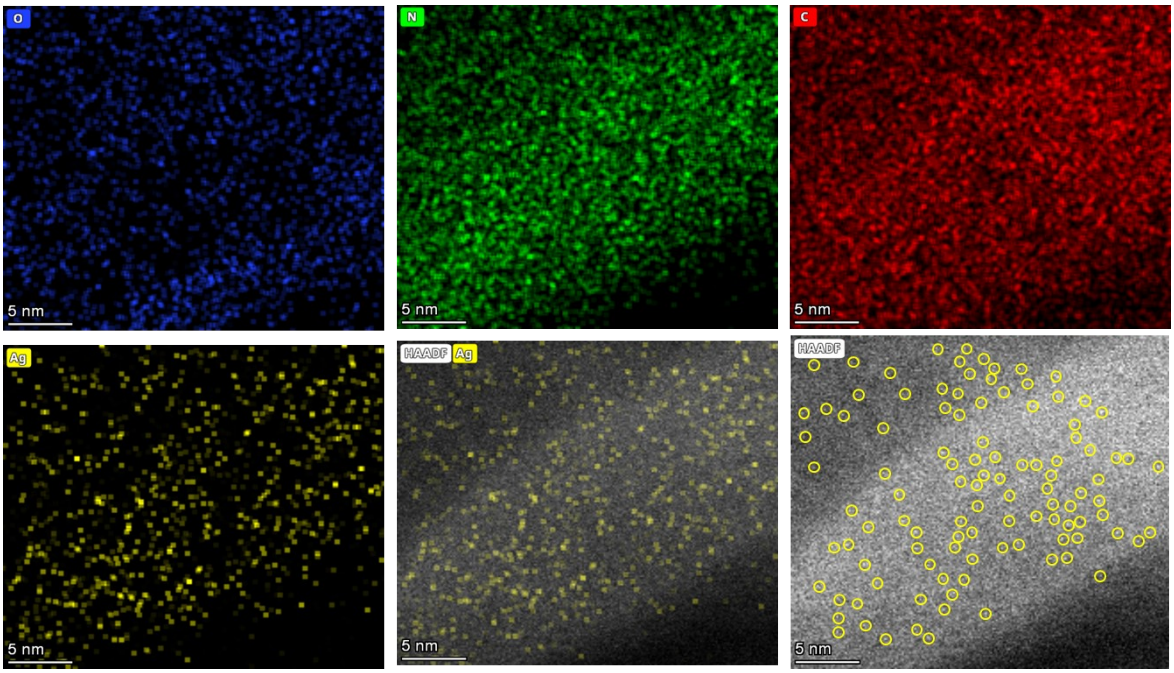

Figure S5. EDS Mapping and HAAD-STEM image of Ag-PCN.

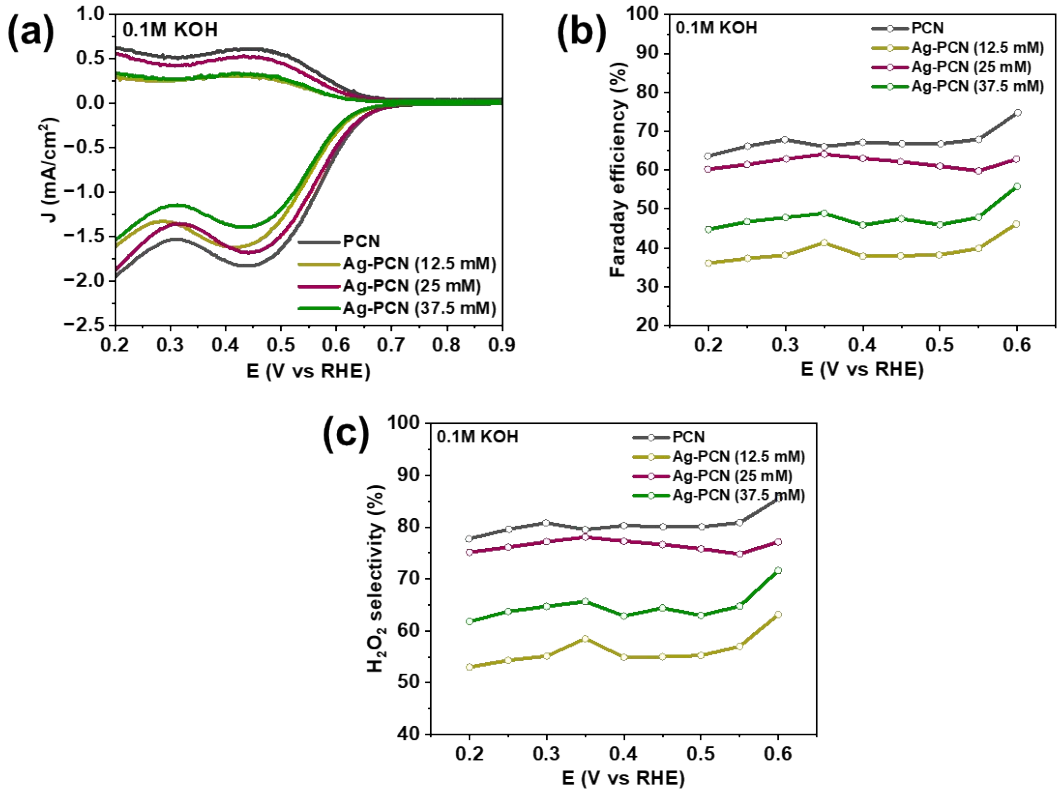

Figure S6. H_2O_2 electroproduction in 0.1M KOH (a) LSV at 1600 rpm, (b) Number of electron transfer, and (c) H_2O_2 selectivity for PCN and Ag-PCN with different compositions.

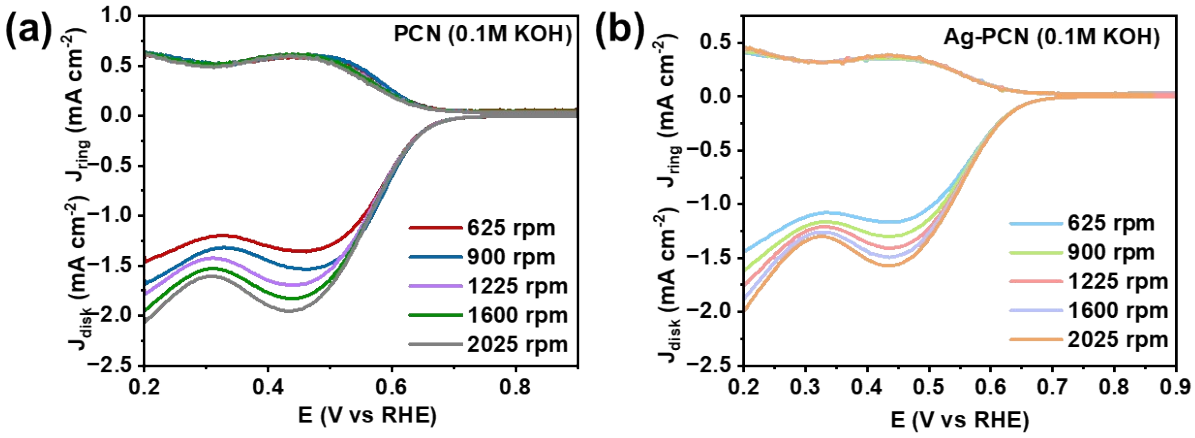

Figure S7. LSV at different rotation rates in 0.1M KOH for (a) PCN , and (b) Ag-PCN.

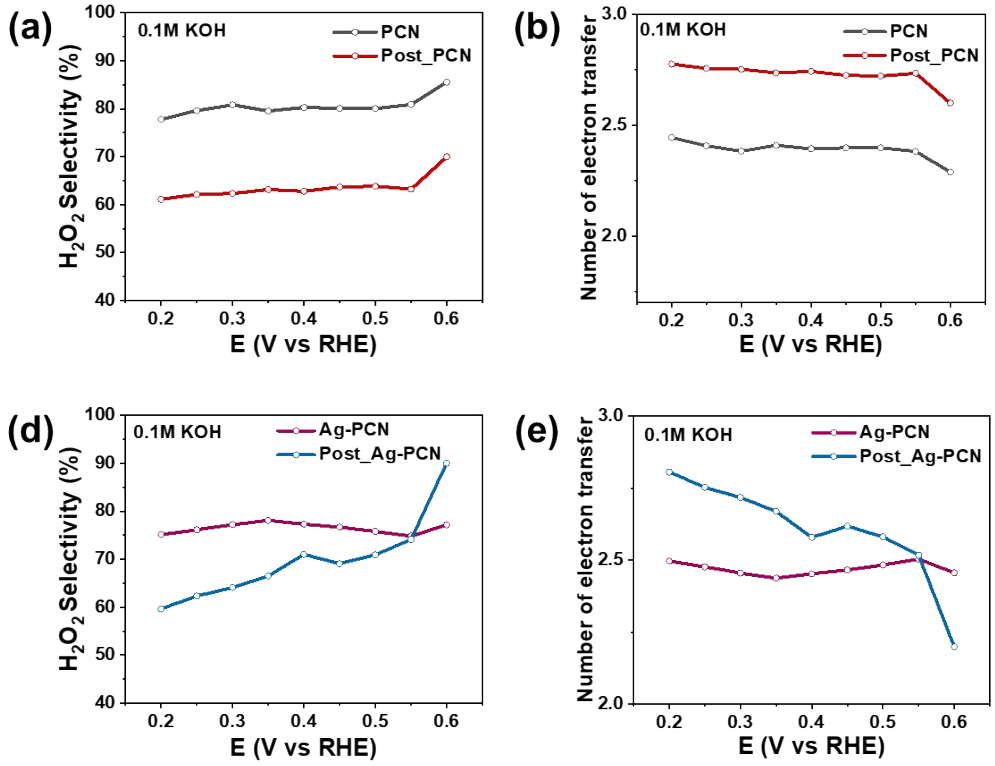

Figure S8. (a) H_2O_2 production selectivity of PCN before after 10h stability, (b) Number of electron transfer in PCN before after 10h stability test, (c) H_2O_2 production selectivity of Ag-PCN before after 18h stability test, (d) Number of electron transfer in Ag-PCN before after 18h stability test in 0.1MKOH in 0.2-0.6 potential verses RHE.

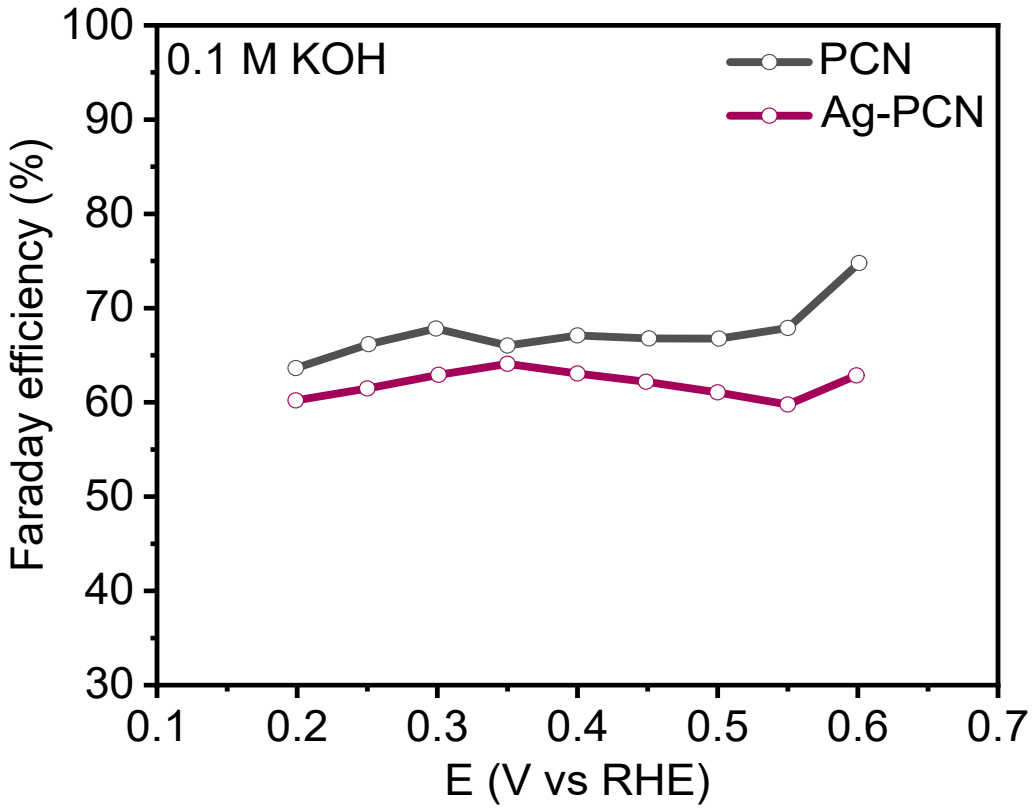

Figure S9. (a) Faradic efficiency (FE) of PCN and Ag-PCN in 0.1KOH.

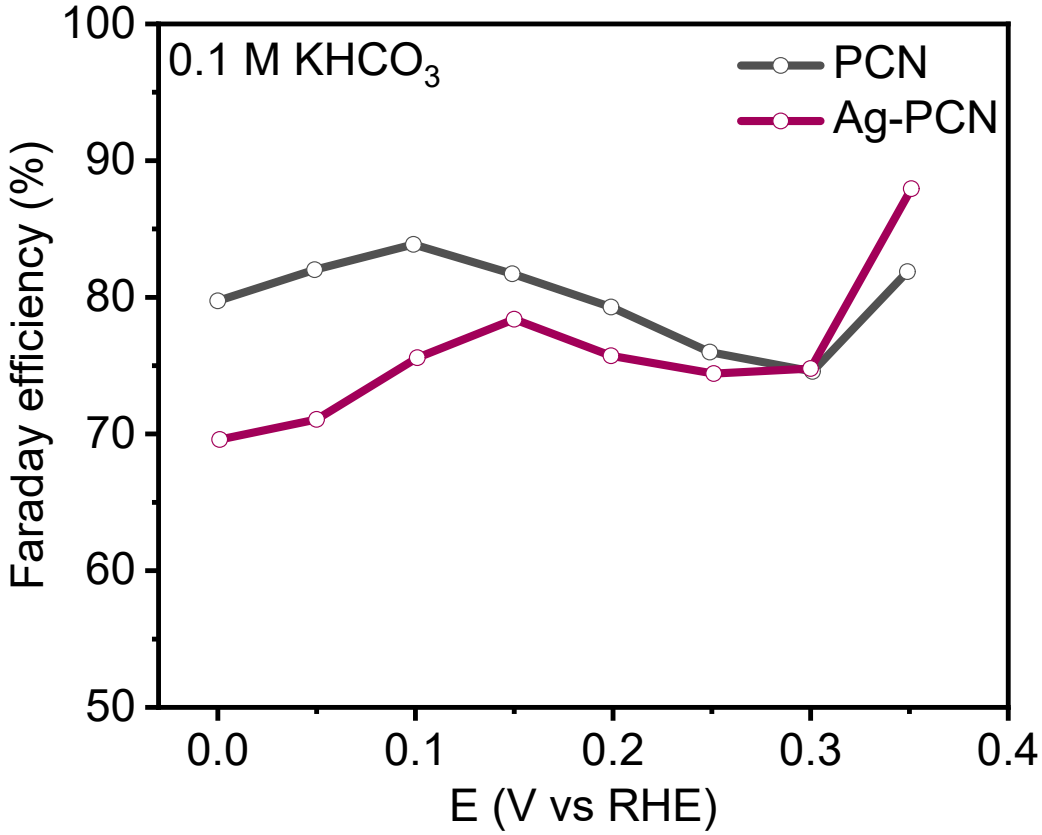

Figure S10. (a) Faradic efficiency (FE) of PCN and Ag-PCN in 0.1$KHCO_3$.

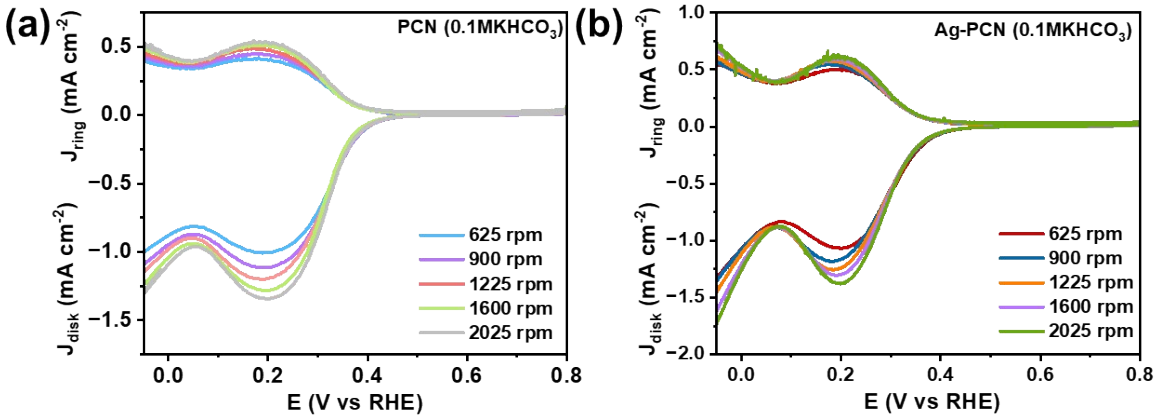

Figure S11. LSV at different rotation rates in 0.1M $KHCO_3$ for (a) PCN, and (b) Ag-PCN.

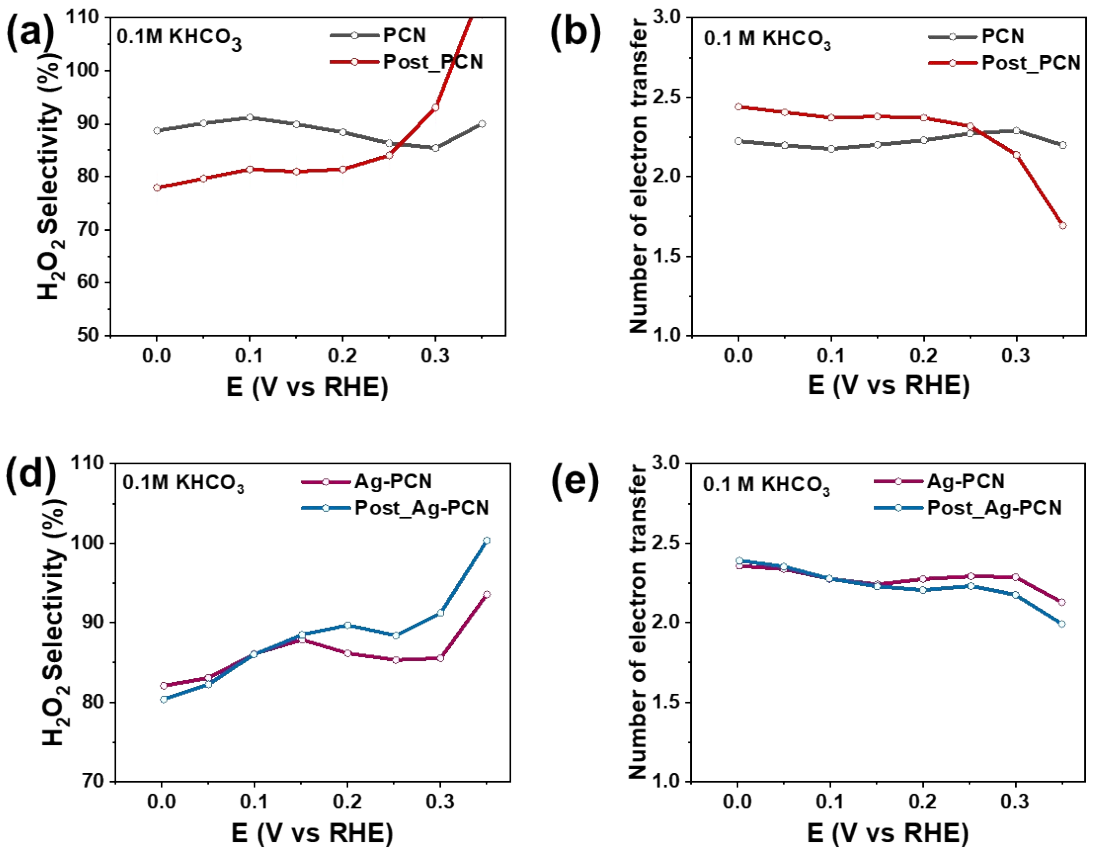

Figure S12. (a) H_2O_2 production selectivity of PCN before after 60h stability, (b) Number of electron transfer in PCN before after 60h stability test, (c) H_2O_2 production selectivity of Ag-PCN before after 60h stability test, (d) Number of electron transfer in Ag-PCN before after 60h stability test in 0.1M$KHCO_3$ in 0.-0.35 potential verses RHE.

Table S1. PCN and Ag-PCN weight before and after one-week chemical stability tests.

Catalyst	**Initial Weight (mg)**	**Weight after one week in 3% H_2O_2**
PCN	70	63 (10% loss)
Ag-PCN	70	69 (1% loss)

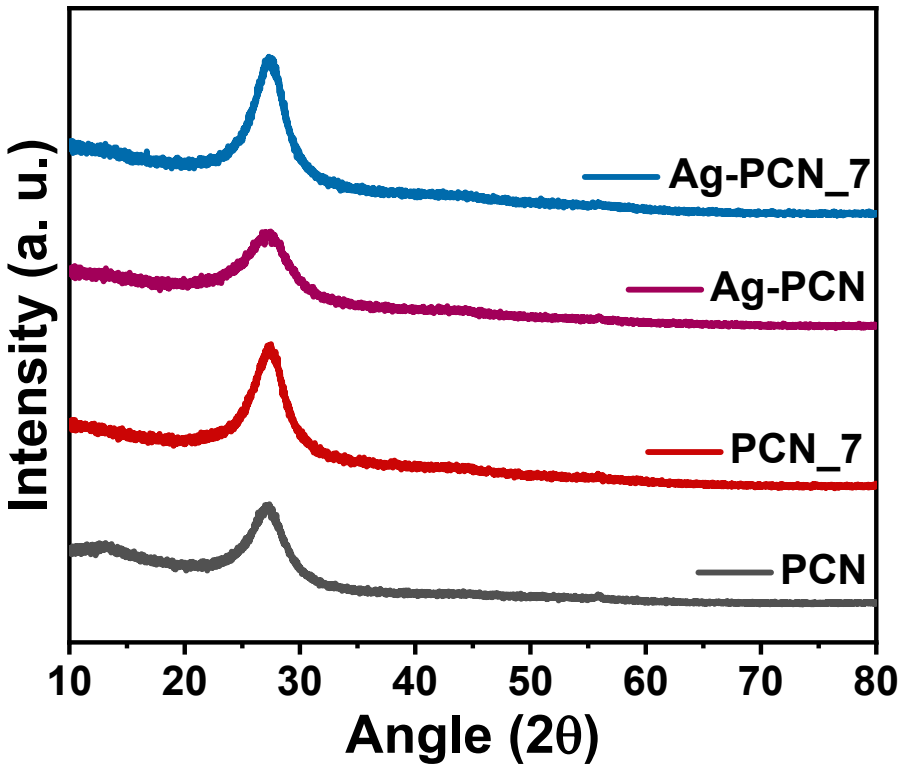

Figure S13. XRD spectra of PCN and Ag-PCN before and after one-week chemical stability test in 3% H_2O_2

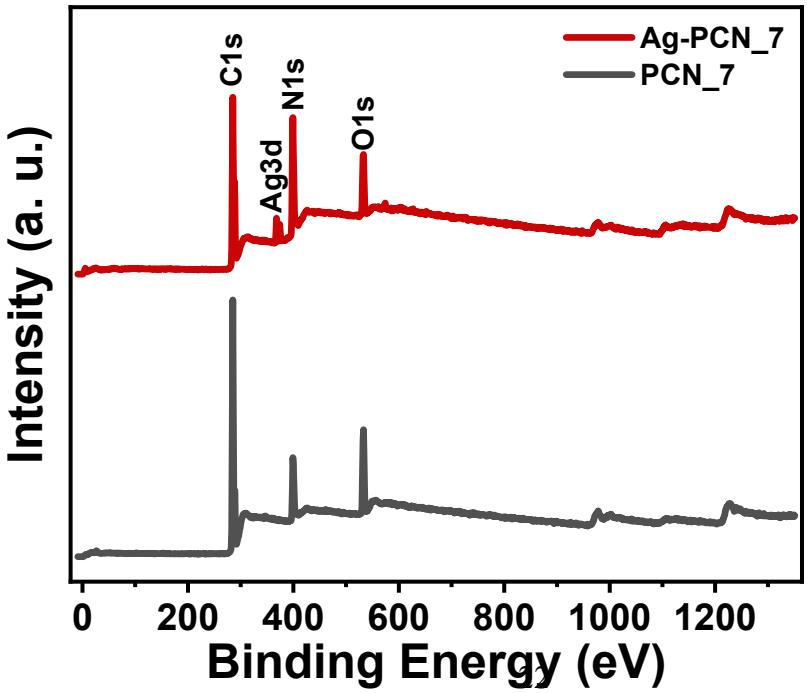

Figure S14. XPS survey spectra of PCN and Ag-PCN before and after one-week chemical stability test in 3% H_2O_2

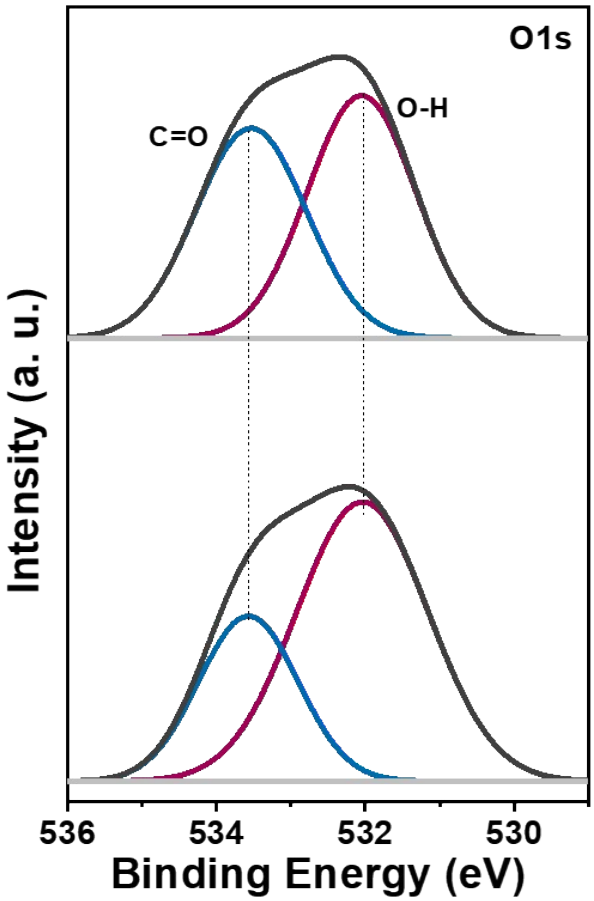

Figure S15. High resolution O1s spectra of Ag-PCN before and after one-week chemical stability test in 3% H_2O_2.

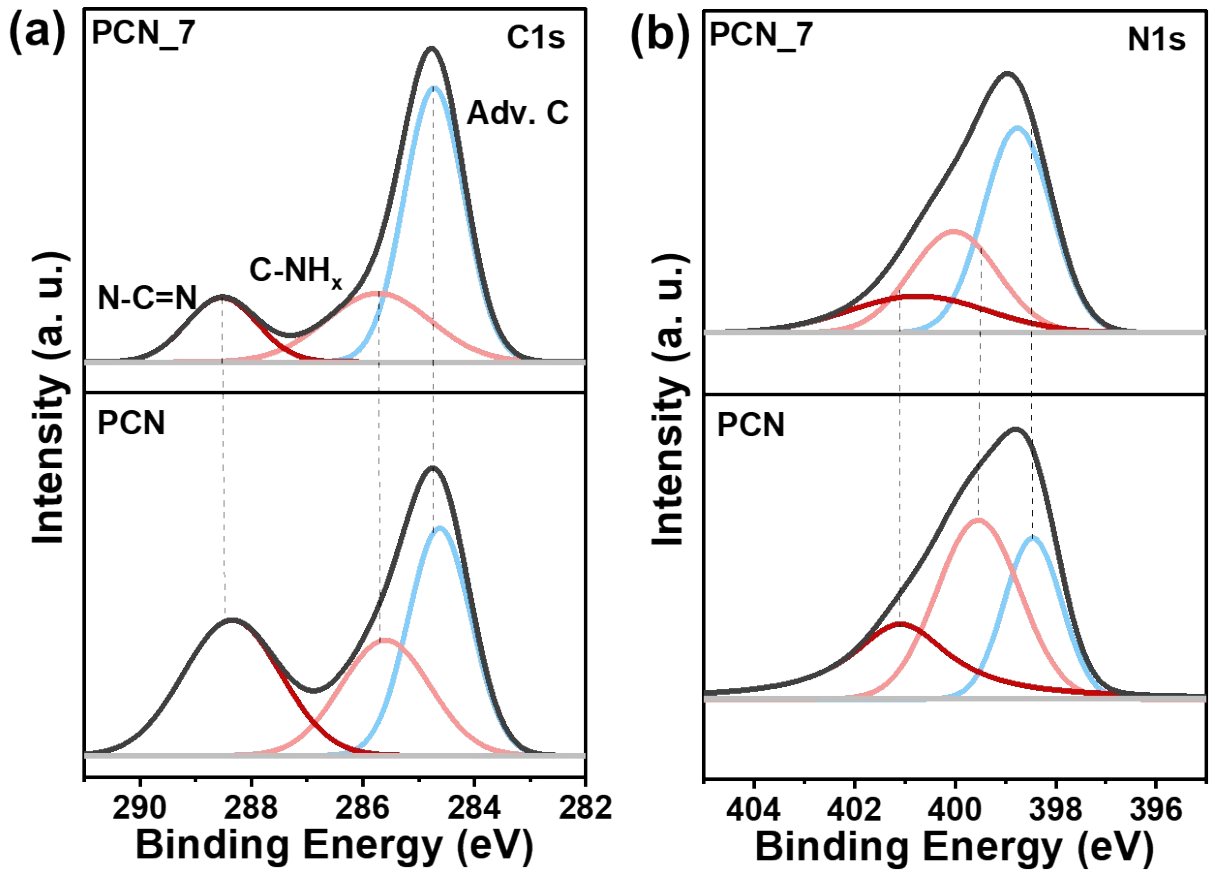
(a)
PCN_7
C1s
Adv. C
C-NHx
N-C=N
PCN
Intensity (a. u.)
290
288
286
284
282
Binding Energy (eV)
(b)
PCN_7
N1s
PCN
Intensity (a. u.)
404
402
400
398
396
Binding Energy (eV)

Figure S16. High resolution C1s and N1s spectra of PCN before and after one-week chemical stability test in 3% H_2O_2.

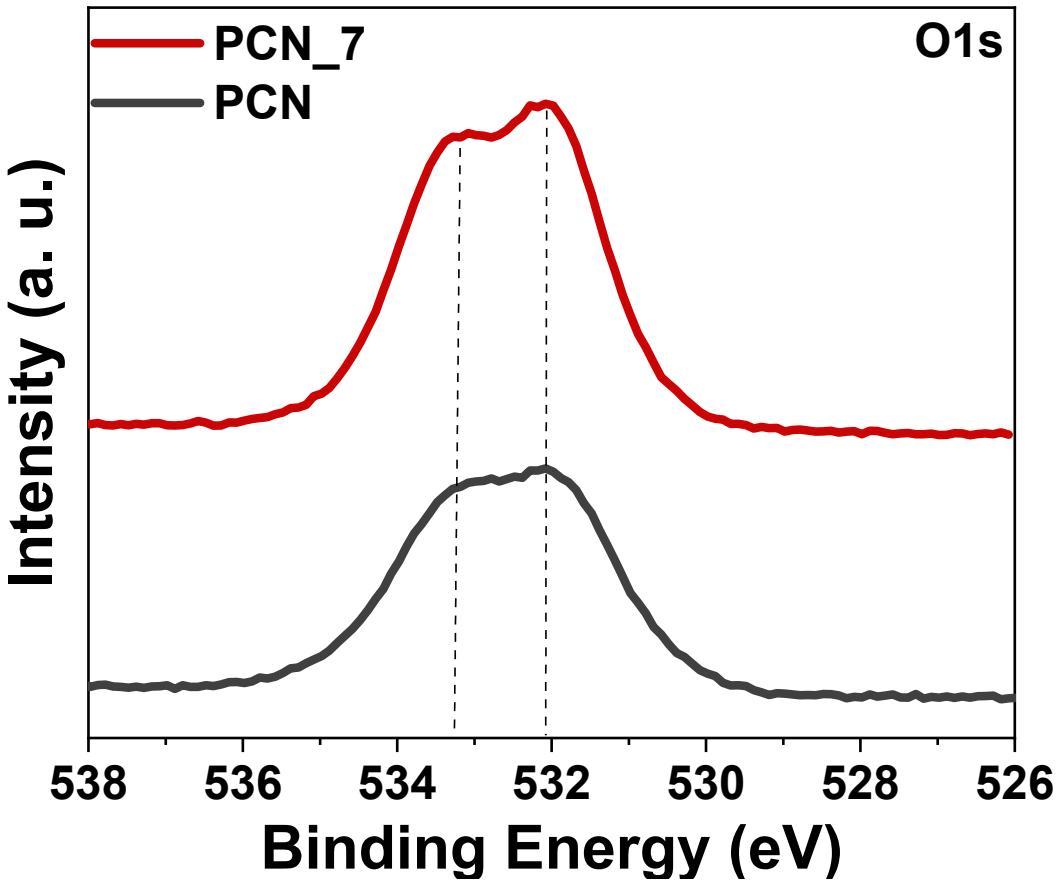

Figure S17. High resolution O1s spectra of PCN before and after one-week chemical stability test in 3% H_2O_2.

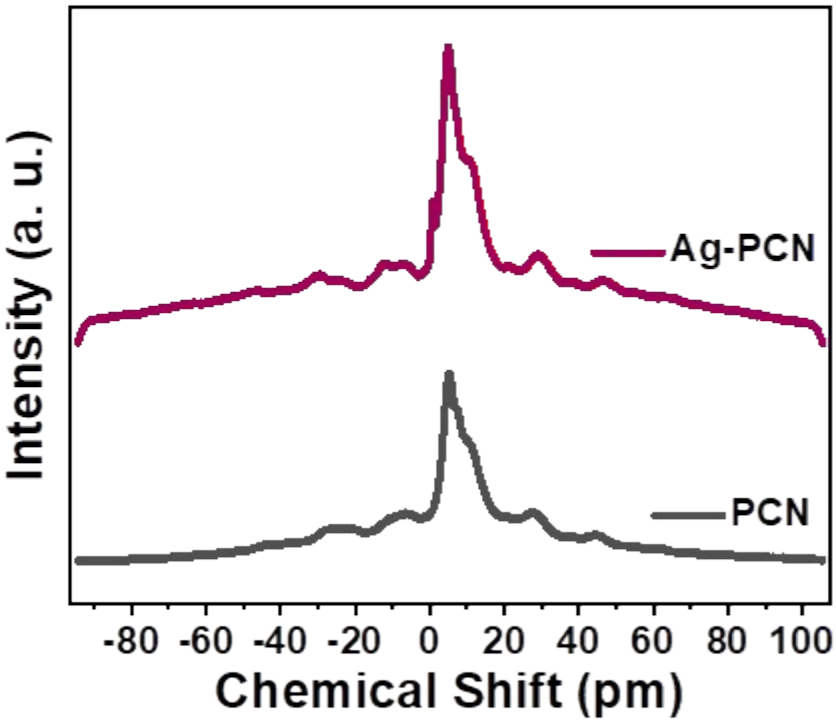

Figure S18. [1]HNMR spectra of PCN and Ag-PCN.

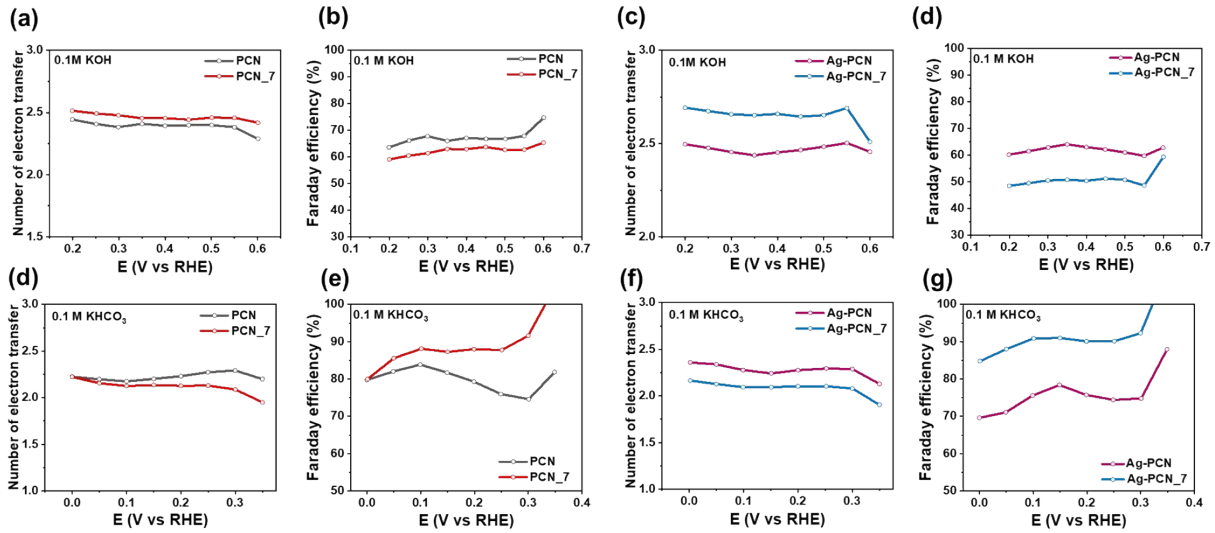

Figure S19. Number of electro transfer before and after one week stability test in 3% H_2O_2 for (a) PCN and PCN_7 in 0.1M KOH, (b) Ag-PCN and Ag-PCN_7 in 0.1M KOH, (c) PCN and PCN_7 in 0.1M $KHCO_3$, and (d) Ag-PCN and Ag-PCN_7 in 0.1M KHC

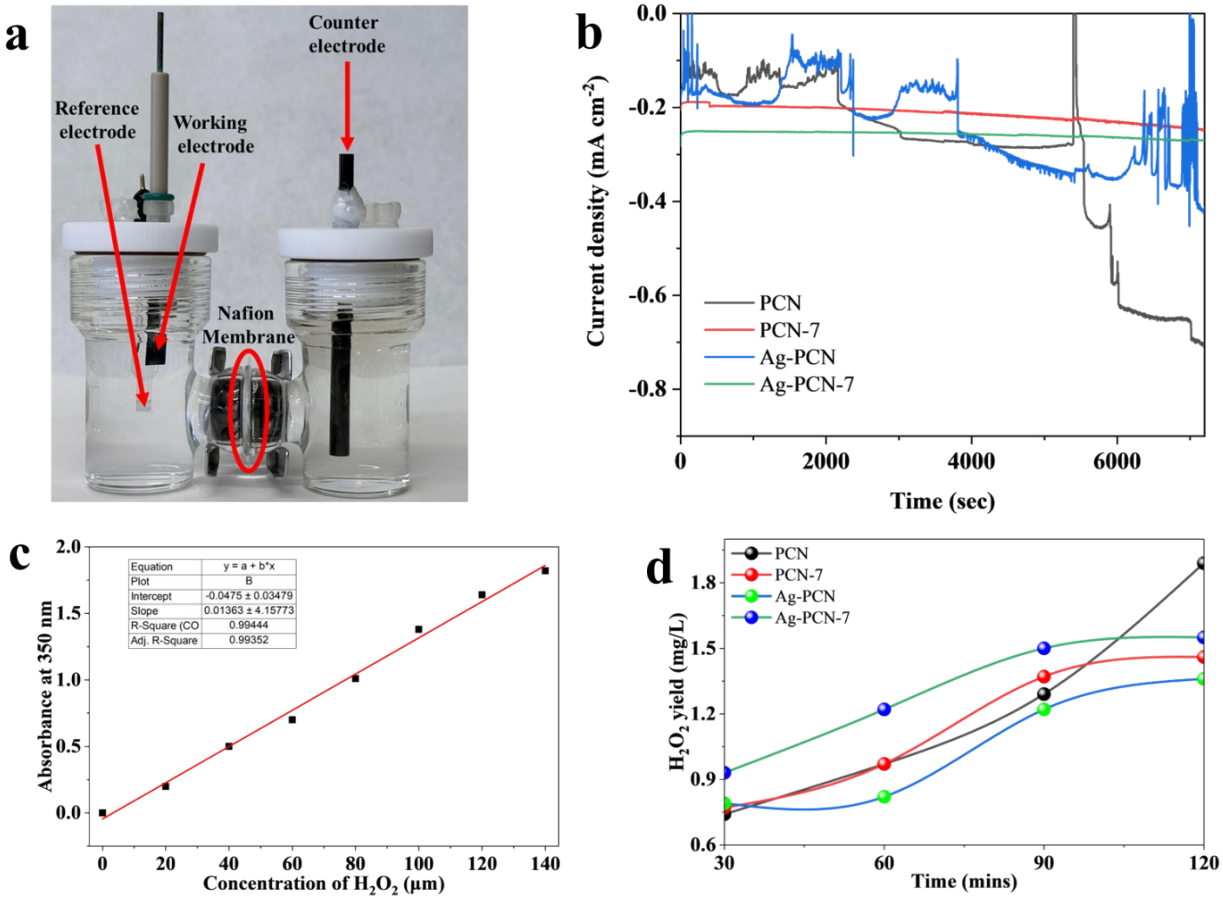

Figure S20. a. Photograph of two compartment H-type electrochemical cell, b. Chronoamperometry test of PCN, PCN-7, Ag-PCN, and Ag-PCN-7, c. H_2O_2 calibration curve for the UV-Vis spectrophotometric method and the measured H_2O_2 concentration, d. Experimentally measured H_2O_2 concentration

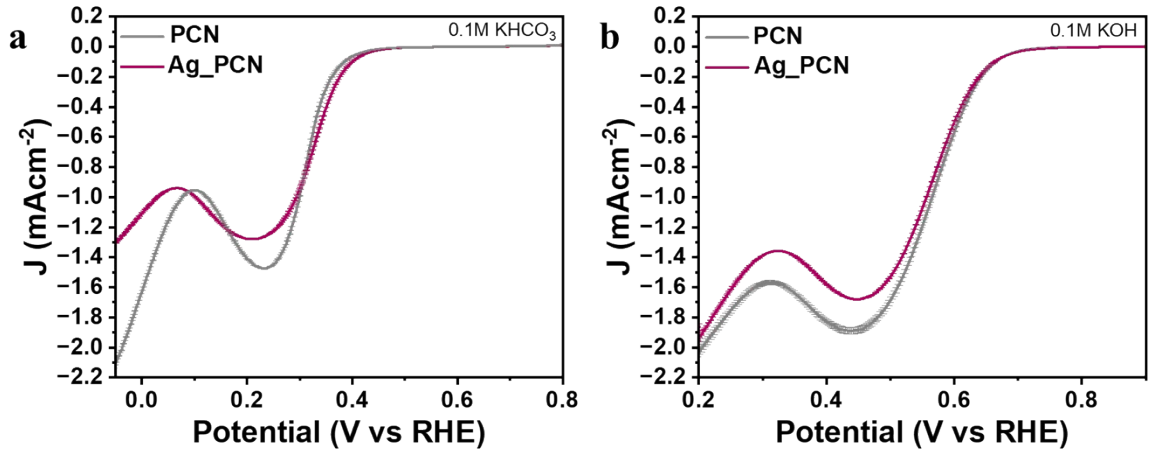

Figure S21. LSV curves with error bars representing the standard deviation from two independent measurements (a) PCN and Ag-PCN in 0.1 M $KHCO_3$ and (b) 0.1M KOH

Supporting Information

Table S2. Comparison of electrochemical H_2O_2 production metrics for Ag-PCN with state-of-the-art single-atom catalysts

Materials	Matrix	Selectivity (%)	Faradaic Efficiency (%)	Electrolyte	Ref
PCN	*Polymeric carbon nitride*	*82*	*75*	*0.1M KOH*	*This work*
PCN		*80*	*70*	*0.1M $KHCO_3$*	
Ag-PCN		*80*	*70*	*0.1M KOH*	
Ag-PCN		*70*	*88*	*0.1 M $KHCO_3$*	
CNNS	$g\text{-}C_3N_4$ nanosheets	61	-	0.1M PBS	14
$Ni_{0.10}$ SA/CNNS		98	97		
$Mn_{0.10}$ SA/CNNS		95	-		
$Zn_{0.10}$ SA/CNNS		93	-		
$Cu_{0.10}$ SA/CNNS		90	-		
$Fe_{0.10}$ SA/CNNS		86	-		
$Co_{0.10}$ SA/CNNS		76	-		
CNNs	$g\text{-}C_3N_4$ nanosheets	76	60	0.1M PBS	15
K-Co/CNNs		97	91		
CoNC-O	N doped C	88.5	-	0.1M $HClO_4$	

[#] Equal contribution

CoNC-O		79	-	0.1M PBS	16
$Pt_{0.21}$/CN	g-C_3N_4 nanosheets	98	96	0.1M KOH	17
Ni-N_4-O	N doped C	95	-	0.1M KOH	18
g-C3N4/CQDs-X	g-C3N4	95	-	0.1M KOH	19
Mn-CN/C	Carbon dots	90	-	0.1M KOH	20
NiSA-NC	N doped C	81	-	0.1M Na2SO4	21
Cu/NCNSs	N doped C nanosheets	76	-	0.1M PBS	22
Co_1/NG(O)	N doped graphene	82	-	0.1M KOH	23
InSAs/NSBC	N,S and B doped carbon nanorods	95.4	-	0.1M KOH	24
		92	-	0.1M PBS	
O-C(Al)	MOF	95		0.1M NaOH	25
		90	N.A	0.1M PBS	

Supporting Information

Table S3. Comparison of chemical and electrochemical stability

Catalyst	Type of test	Material Degradation	Selectivity		Electrolyte	Ref
			Initial	Final		
PCN	*CA-10 hours*	-	85	70	*0.1M KOH*	*This work*
Ag-PCN	*CA-18 hours*	-	77	90	*0.1M KOH*	
PCN	*CA-60 hours*	-	90	100	*0.1M $KHCO_3$*	
Ag-PCN	*CA-60 hours*	-	94	100	*0.1M KHCO3*	
PCN	*Chemical stability (Soaked in 3% H_2O_2 for 1 week)*	*9%*	*85*	*79*	*0.1M KOH*	
PCN			*90*	*100*	*0.1M $KHCO_3$*	
Ag-PCN		*1%*	*77*	*75*	*0.1M KOH*	
Ag-PCN			*93*	*100*	*0.1M $KHCO_3$*	
$Ni_{0.10}$ SA/CNNS	CP-16hrs	-	98	96.6-98.8	0.1M PBS	26
$Ni_{0.10}$ SA/CNNS	Physical stability- The catalyst ink was stored for 68 days and used again	NA	98	94		

[#] Equal contribution

$Pt_{0.21}$/CN	40000 cycles	NA	98	94	0.1M KOH	27

Table S4. The yield rate of H2O2 produced by H-cell experiments

Catalyst	Type of cell	Electrolyte	H2O2 productivity (mol gcat-1 h-1)	Faradaic Efficiency	Reference
PCN	H-Cell	0.1M $KHCO_3$	0.00981	73.54	Our Work
PCN-7			0.0101475	54.66	
Ag-PCN			0.0104805	~100	
Ag-PCN-7			0.01233	53.08	
Ni-N_4O	H-Cell	0.1M PBS	0.3168	-	28
InSAs/NSBC	PEMFC	0.1M KOH	6.49	77.3	29
		0.1M PBS	6.71	80	
COF-366-Co	H-shape electrolyzer	0.1M KOH	0.909	82	30
O-C(Al)	H-Cell	0.5M Na2SO4	0.026	92	31

[#] Equal contribution

Table S5: Free energy calculations values:

OOH Adsorption Sites	**Adsorption Energy E_{ads} (eV)**	**ΔZPE**	**TΔS**	**Adsorption Free Energy (eV)**	
				U= 0.0 V	**U= 0.7 V**
OOH on C atom of pristine C_3N_4	-2.24	0.469	0.146	-1.91	-1.21
OOH on C atom of Ag@C_3N_4	-2.03	0.472	0.143	-1.70	-1.0
OOH on Ag atom of Ag@C_3N_4	-1.69	0.430	0.194	1.45	-0.75

Table S6: Band gap values before and after *OOH intermediate adsorption:

System	**Band Gap (eV)**
Pristine Layer	1.18
Ag-PCN Layer	1.17
topC@Ag-PCN	1.17
topAg@Ag-PCN	0.32

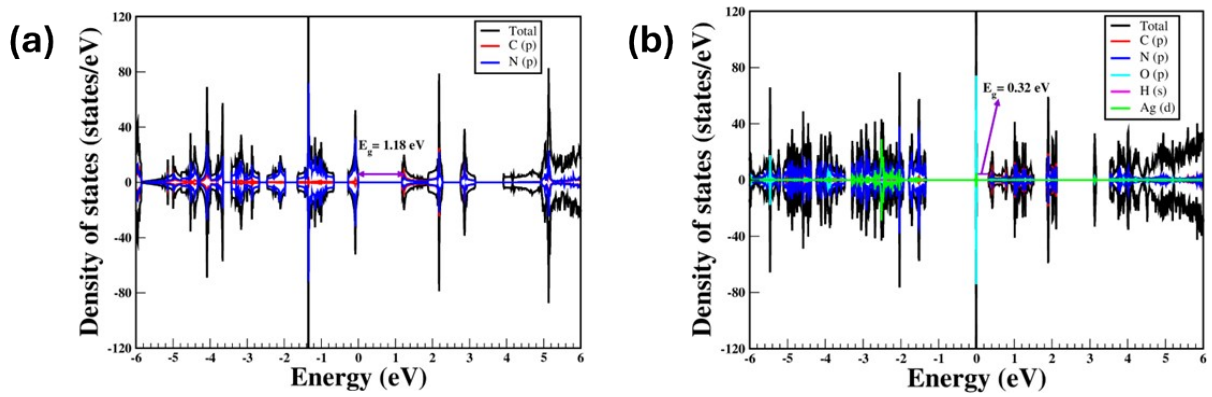

Figure S22. Spin-polarized projected density of states (PDOS) plot of (a) pristine C_3N_4 monolayer, (b) after *OOH adsorption on top of Ag inside C_3N_4 layer. Fermi energy is shifted at zero eV.

References

1. Hohenberg, P.; Kohn, W. Phys. Rev.1964,136, B864–B871.
2. Kohn, W.; Sham, L. J. Phys. Rev.1965,140, A1133–A1138.
3. Perdew, J. P.; Burke, K.; Ernzerhof, M. Phys. Rev. Lett.1996,77, 3865–3868.
4. Blöchl, P. E. Projector augmented-wave method. Phys. Rev. B1994,50, 17953–17979.24.
5. Kresse, G.; Furthmüller, J. Phys. Rev. B1996, 54, 11169–11186.
6. Kresse, G.; Furthmüller, Comput. Mater. Sci. 1996, 6 15-50.
7. Monkhorst, H. J.; Pack, J. D. Phys. Rev.B1976,13, 5188-5192.
8. S. Grimme, J. Antony, S. Ehrlich, H. Krieg, J. Chem. Phys. 2010, 132, 154104.
9. Momma, K; Izumi, F. J. Appl. Crstallogr. 2011, 44, 1272-1276

10. J. K. Nørskov, T. Bligaard, A. Logadottir, J. R. Kitchin, J. G. Chen, S. Pandelov and U. Stimming, *J Electrochem Soc*, 2005, 152, J23.

11. J. K. Nørskov, J. Rossmeisl, A. Logadottir, L. Lindqvist, J. R. Kitchin, T. Bligaard and H. Jónsson, *Journal of Physical Chemistry B*, 2004, 108, 17886–17892.

12. H. A. Hansen, J. Rossmeisl and J. K. Nørskov, *Physical Chemistry Chemical Physics*, 2008, 10, 3722.

13. F. Xiang, X. Zhao, J. Yang, N. Li, W. Gong, Y. Liu, A. Burguete-Lopez, Y. Li, X. Niu and A. Fratalocchi, *Advanced Materials*, DOI:10.1002/adma.202208533.

14. Yang H, Ma F, Lu N, Tian S, Liu G, Wang Y, Wang Z, Wang D, Tao K, Zhang H, Peng S. Nanoscale Horizons. 2023;8(5):695-704.

15. Wang Y, Yang H, Lu N, Wang D, Zhu K, Wang Z, Mou L, Zhang Y, Zhao Y, Tao K, Ma F. Nanoscale. 2023;15(47):19148-58.

16. Lu T, Liu Y, Li Y, Chen J, Chen S, Liao X, Xia W, Zhou T, Wang W, Chen Z, Huang R. Applied Catalysis B: Environment and Energy. 2025 15; 365:124949.

17. Yang H, Lu N, Zhang J, Wang R, Tian S, Wang M, Wang Z, Tao K, Ma F, Peng S. Carbon Energy. 2023 Sep;5(9):e337.

18. Liu Z, Zhang B, Liu Y, Wang C, Ye C, Yang W. A Journal of Materials Chemistry A. 2025;13(15):10683-93.

19. H. Yang, F. Ma, N. Lu, S. Tian, G. Liu, Y. Wang, Z. Wang, D. Wang, K. Tao, H. Zhang and S. Peng, *Nanoscale Horizons*, 2023, **8**, 695–704.

20. Y. Wang, H. Yang, N. Lu, D. Wang, K. Zhu, Z. Wang, L. Mou, Y. Zhang, Y. Zhao, K. Tao, F. Ma and S. Peng, *Nanoscale*, 2023, **15**, 19148–19158.

21. T. Lu, Y. Liu, Y. Li, J. Chen, S. Chen, X. Liao, W. Xia, T. Zhou, W. Wang, Z. Chen, R. Huang and H. Wang, *Appl. Catal. B Environ.*, 2025, **365**, 124949.

22. H. Yang, N. Lu, J. Zhang, R. Wang, S. Tian, M. Wang, Z. Wang, K. Tao, F. Ma and S. Peng, *Carbon Energy*, 2023, **5**, 1–12.

23. Z. Liu, B. Zhang, Y. Liu, C. Wang, C. Ye and W. Yang, *J. Mater. Chem. A*, 2025, **13**, 10683–10693.

24. Y. Wang, Z. Yang, C. Zhang, Y. Feng, H. Shao, J. Chen, J. Hu and L. Zhang, *Ultrason. Sonochem.*, 2023, **99**, 106582.

25. Y. Zeng, X. Tan, Z. Zhuang, C. Chen and Q. Peng, *Angew. Chemie - Int. Ed.*, DOI:10.1002/anie.202416715.

26. Z. Lin, J. Lohwacharin, Y. Li and Y. Wang, *J. Colloid Interface Sci.*, DOI:10.1016/j.jcis.2025.138814.

27. C. Ye, Y. Zhou, H. Li and Y. Shen, *Green Chem.*, 2023, **25**, 3931–3939.

28. E. Jung, H. Shin, B. H. Lee, V. Efremov, S. Lee, H. S. Lee, J. Kim, W. Hooch Antink, S. Park, K. S. Lee, S. P. Cho, J. S. Yoo, Y. E. Sung and T. Hyeon, *Nat. Mater.*, 2020, **19**, 436–442.

29. E. Zhang, L. Tao, J. An, J. Zhang, L. Meng, X. Zheng, Y. Wang, N. Li, S. Du, J. Zhang, D. Wang and Y. Li, *Angew. Chemie - Int. Ed.*, DOI:10.1002/anie.202117347.

30. Q. Yang, W. Xu, S. Gong, G. Zheng, Z. Tian, Y. Wen, L. Peng, L. Zhang, Z. Lu and L. Chen, *Nat. Commun.*, 2020, **11**, 1–10.

31. C. Liu, H. Li, F. Liu, J. Chen, Z. Yu, Z. Yuan, C. Wang, H. Zheng, G. Henkelman, L. Wei and Y. Chen, *J. Am. Chem. Soc.*, 2020, **142**, 21861–21871.